Thermophones using carbon nanotubes and alternative nanostructures for high power sound generation and noise cancellation

Ali E. Aliev[1]

Alan G. MacDiarmid NanoTech Institute, University of Texas at Dallas, USA

ABSTRACT

There is a large promise for thermophones in high power sonar arrays, flexible loudspeakers and noise cancellation devices. The freestanding aerogel-like carbon nanotube sheet as a thermoacoustic (TA) heat source demonstrates so far the best performance. However, the limited accessibility of large size free standing carbon nanotube sheets and other even more exotic materials published recently, hampers the field. I present here new alternative materials for TA heat source with high energy conversion efficiency, additional functionalities, environmentally friendly and cost effective production technologies. I discuss the TA performance of alternative nanoscale materials and compare their spectral and power dependencies of sound pressure in air. The study presented here focuses on engineering of thermal gradients in the vicinity of nanostructures and subsequent heat dissipation processes from the interior of encapsulated thermoacoustic projectors. Applications of TA projectors for high power SONAR arrays, sound cancellation, and optimal thermal design, regarding enhanced energy conversion efficiency, are discussed.

Keywords: Thermoacoustic Sound generation, 21.7 Vibration excitation by mechanical and electrical sources

1. INTRODUCTION

Thermoacoustic (TA) sound generation using nanoscaled materials like carbon nanotube (CNT) sheets, graphene films and mechanically suspended nanoscale metallic wires recently attracted much research interest. An efficient TA sound source requires low heat capacity per unit area and efficient heat exchange with the surrounding medium. Among the studied materials (carbon nanotubes [1-4], graphene [5-8], PEDOT: PSS and ITO films [9, 10], porous silicone [11] and metal wire arrays [12]) the aerogel density CNT sheets demonstrate the best performance. Table 1 compares the performance of some nanoscale materials applied for TA heat source. Indeed, the small heat capacity, high mechanical strength, and extremely high accessible surface area makes the freestanding aerogel CNT sheet one of the best heat source material for TA applications. The aerogel structure of freestanding CNT sheets makes the gas heating process more of a volume rather than of a surface type. Moreover, the high alignment of CNTs, provided by dry-state withdrawing technology, is another crucial features enhancing the efficiency of sound generation; in randomly deposited CNTs or network of nanowires, the components aligned perpendicular to the current flow direction do not contribute to sound production.

Transparent CNT sheets, which have the density of air and the electrical conductivity of metals [13], have been demonstrated to be suitable TA sources for use in harsh gaseous environments [1] and underwater [2]. CNT films open to the propagating medium can generate sound over a wide frequency range (1-10^5 Hz). The variation of temperature and pressure in the vicinity of an open CNT heater induces sound wave propagation in the surrounding medium. Increasing the thermal gradient created between the surface of CNT sheet and surrounding medium within the thermal diffusion length (l_d=$(2\alpha/\omega)^{1/2}$, where α is the thermal diffusivity and ω is the angular frequency of temperature modulation, results in increased sound pressure intensity. A higher applied power P_h produces an increased temperature gradient (Eq.12 in [4]) and subsequently higher sound pressure and Carnot's efficiency. Despite the extremely low heat capacity of aerogel density CNT sheet, the small but finite heat capacity of air accompanied by its low thermal conductivity leads to an accumulation of heat in the vicinity of the heater.

[1] Ali.Aliev@utdallas.edu

This elevated background temperature decreases the efficiency of the TA projector. The heat dissipation conditions are more severe for low surface area graphene and other continues 2D films like PEDOT:PSS, ITO films, and metallic films on the surface of porous materials.

Table 1. The comparison of TA sound source performances at frequency most sensitive to the human ear, f = 3 kHz, T=295 K.

	Heater material	p_{rms}, **Pa**	**SPL, dB**	**η, %**	**Reference**
1	CNT sheet, (25.0 cm^2)	0.117	75	$2x10^{-5}$	Single layer MWNT sheet, D=10 nm, [4]
2	Graphene, #1. (2.25 cm^2) #2. (6.25 cm^2)	0.0045 0.0028	47 43		3-layer graphene suspended on 80% porous PDMS, [8]
3	Graphene, (1.0 cm^2)	0.0115	55	10^{-6}	20 nm thick graphene film on paper, [7]
4	PEDOT:PSS	0.0025	32	10^{-6}	100 nm PEDOT:PSS film on glass substrate, [9]
5	ITO film	0.0028	34	$2x10^{-8}$	100 nm ITO film on PET substrate [12]
6	Al film on porous silicon, P_h=1 W/cm^2, (6.25 cm^2)	0.0147/cm^2 0.00235	57 41		30 nm thin Al film on 10 μm thick nanoporous (70%) silicon, [10]
7	Au film on porous polymeric substrate, (~10 cm^2)	0.034	64		40 nm thin Au film on 14 μm thick porous (5%) hydrogel substrate, [14]
8	Al film on polyimide substrate (4 cm^2)	0.0019	39.5		40 nm Al film on 75 μm polyimide substrate, [15]
9	Suspended metal wire array (17.5 cm^2)	0.035	65		3 μm wide and 30 nm thick Al nanowires, [11]

* The sound pressure, p_{rms} and sound pressure level, SPL (re 20 μPa) were normalized to f = 3 kHz, P_h=1W, and r = 3 cm assuming linear dependencies of $p(f)$, $p(1/r)$ and $p(P_h)$ from original plots in presented references. The energy conversion efficiency η for CNT sheet is shown for P_h=1W, while for others, as were mentioned in references. The parenthesis in first column show the surface area of tested samples.

A complete characterization of thermodynamic properties of suitable nanostructured materials for TA transductions is challenging and needs very sophisticated techniques: Thermal atomic force microscope, 3-omega self-heating technique, suspended microfabricated device, micro-Raman and so on. However, the slope of sound pressure plotted versus frequency and applied ac power can explicitly characterize the heat source performance.

I address here the thermal, acoustical and energy conversion issues in TA projectors by seeking alternative heat source materials providing additional functionality, are environmentally friendly and have cost effective production technologies. I systematically investigate the spectral and applied ac power response for materials with different thickness, porosity and heat capacity and analyze the effects of heat accumulation on the fundamental efficiency of TA sound generation.

2. RESULTS

For the frequency region f < 100 kHz, the linear amplitude-frequency response of a TA device results from the negligible heat capacity of the nanoscaled heat source, C_h [1, 4]:

$$p_{rms} = \frac{f}{2\sqrt{2}C_p T_0} \cdot \frac{1}{r} \cdot P_h , \quad (1)$$

where C_p is the heat capacity of the gas, T_0 is the temperature of the surrounding gas, r is the distance to the microphone and P_h is the power applied to the heat source. This dependency was proved for many carbon nanotube based freestanding sheets, both single-walled and multi-walled. For heat source structures with larger diameter of constituent fibers, flakes or films, the heat capacity of the heater should be taken in to account. The corresponding slope of sound pressure versus frequency for thermally inert TA heat sources is gradually declined towards $p_{rms} \sim f^{0.5}$ [16]:

$$p_{rms} = \left[\frac{\sqrt{\alpha}\rho_0}{2\sqrt{\pi}T_0 C_h} \right] \frac{\sqrt{f}}{r} P_h , \qquad (2)$$

where C_h is the heat capacity per unit area of the heat source and α is the thermal diffusivity of gas and ρ_0 is the density of gas. Hence, one can make certain conclusions on the structural nature of the TA heater from the obtained $p_{rms}(f)$ and $p_{rms}(P_h)$ taken at different frequencies. Below, the performance of TA devices based on different nanoscaled materials is studied using $p_{rms}(f)$ and $p_{rms}(P_h)$ slopes. Very important additional information on heat exchange and accumulation can be extracted by monitoring the temperature on the surface of the heater.

Improvement to the homogeneity, reduced heat capacity and enhanced heat exchange coefficient with surrounding gas of new nanoscaled heat sources is the major challenge for boosting the temperature modulation gradient, which governs efficiency. The bundling of individual CNTs in large (50-100) ropes creates dramatic current redistribution in the CNT sheet: current flows mainly along the bundles. Only a small fraction (< 10%) of nanotubes on the surface of those bundles can effectively interact with surrounding gas and contribute to the heat exchange process. Nanotubes in small bundles and single nanotubes are at much lower temperatures due to higher thermal exchange efficiency (due to the high surface-to-volume ratio and lower heat capacitance). The thermal inertia of large bundles increases the average temperature of the surrounding gas and decreases the overall efficiency of the Carnot's cycle. Thus, we emphasis our search for a nanoscaled heat source which adopts the small heat capacity and high surface area of free-standing CNTs, while less susceptible to the bundling by van der Waals forces than CNTs.

A nanoscaled heat source having a positive temperature coefficient of resistivity (TCR) will be explored to create a desired dynamic redistribution of current pathways. To achieve the metallic conductivity with positive TCR, we search for metal coated organic fibers with diameters of individual fibers higher than 30 nm (no bundling was observed in nanotubes with diameter above ~ 30 nm).

2.1 Free-standing CVD-grown MWNT forest.

The thermoacoustic and photoacoustic responses of as-grown aligned arrays of multiwalled carbon nanotube (MWNT) forest on silicon substrate are suffer a heat transfer from the heated MWNT layer to the substrate. The heat loss to the substrate especially pronounced for short forests, results in low efficiency and sharp frequency dependence of the sound pressure, $f^{1.2}$ [17]. Here I test the TA sound generation ability of freestanding CVD-grown MWNT forest peeled off from the silicon substrate as a whole sheet (3.5x3.5 cm^2). It is well known that the porosity of CVD-grown forest is extremely high, $V_{void}/V_{CNT} > 99\%$ and nanotubes are less bundled than in sheet fabricated by dry-state withdrawal processing. The 250 μm tall freestanding MWNT forest shown in Figure 1(a) has stable 120 Ω resistance after multiple current cycling (initial resistance was 132 Ω). In low frequency region, f < 10 kHz, the forest exhibits a linear sound pressure spectrum as predicted for nanoscale source with negligible heat capacity, Eq.(1). For the specific heat capacity of air C_p=1006 J/kg·K, f = 3 kHz and a distance to microphone of 3 cm, the pressure variation slope obtained using Eq.(1) is p_{rms}=0.117 Pa/W, which is consistent with the $p_{rms}(P_h)$ slope measured for the single freestanding MWNT sheet. However, the 250 μm tall forest having much lower gas access to the inner parts, reducing the heat transfer coefficient β, at increased power creates an accumulation of heat inside the forest. The heat accumulation produces an undesired increase in static background temperature, T_0, and a corresponding decrease of TA sound pressure slope for both $p_{rms}(f)$ and $p_{rms}(P_h)$. The one order lower sound pressure, compared to the aerogel density MWNT sheet, is a direct consequence of reduced heat transfer coefficient. Note, the linear slope of ($p_{rms} \sim f^1$) in Figure 2(a) at low frequencies (f < 10 kHz), for given applied power, is still conserved, indicating the negligible heat capacity of the forest compared to air.

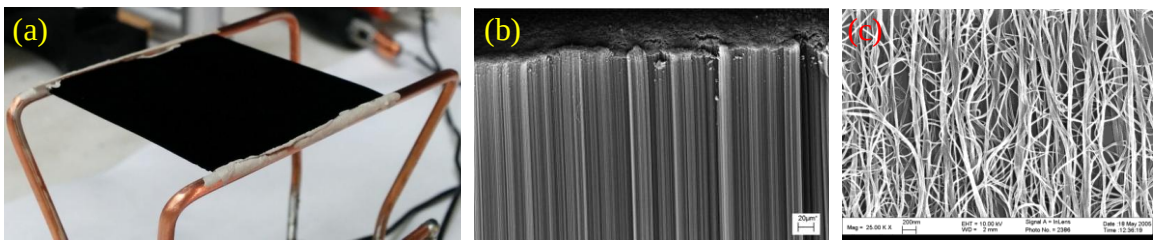

Figure1. (a) The picture of 250 μm tall (3.5x3.5 cm^2) freestanding MWNT forest attached to the copper electrodes by silver paste. (b, c) An SEM image of the forest's side view at increasing magnification.

The clearly visible deviation from linear $p_{rms}(P_h)$ dependence in Figure 2 (b) starts earlier at relatively low applied power. The temperature on the surface of MWNT forest heater, measured using infrared camera MobIR (Wuhan Guide Infrared Technology Co., Ltd.) with preinstalled emissivity of 0.98 (almost perfect black body), shows a strong deviation from linear behavior with further square root dependence at applied ac power above 5 W. The non-linear behavior of $p_{rms}(P_h)$ and $T(P_h)$ in Figure 2(b) is partially resulted by non-linear thermal conductivity behavior of air in vicinity of the heater ($\kappa \sim (T/M)^{1/2}$, for monatomic gases with molar weight M), which is enhanced at high power by black-body radiation from the hot individual nanotubes. We observed the same behavior for a stack of MWNT sheets ($n > 6$) [18].

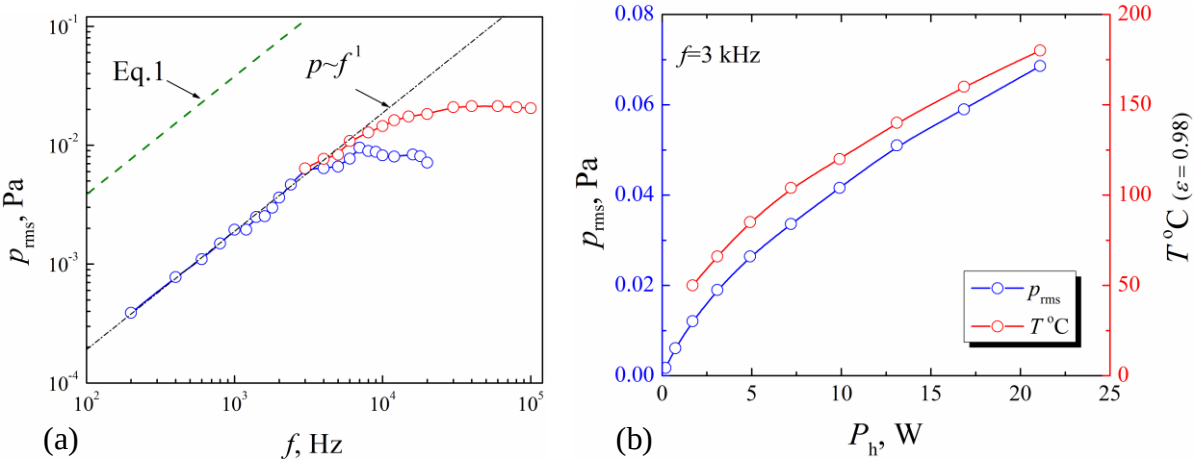

Figure 2. (a) The sound pressure spectra of freestanding MWNT forest (3.5x3.5 cm^2) measured at a distance of 3 cm in open air at T_0=25 °C. The sound pressure is normalized to the applied ac power, P_h=3 W. Open blue circles show the $p_{rms}(f)$ response measured using precision condenser microphone model 7046, (2 Hz–20 kHz) and open red circles, using model 7016, (5 Hz–120 kHz) (ACO Pacific, Inc). The green dashed line show the theoretical line according to Eq.(1). (b) The sound pressure versus applied ac power (open blue circles) measured on the distance r=3 cm, f=3 kHz. The temperature of suspended MWNT forest versus applied power (open red circles) was measured using infrared camera MobIR.

2.2 Highly elastic deformable MWNT sponge.

Developing flexible and deformable devices based on porous materials is of high interest in energy related fields. Here, I demonstrate that CNT sponges consisting of highly porous conductive MWNT networks can serve as a compressible and flexible TA heat sources. The 2x2.5 cm^2 and 1.5x1.5 cm^2 sponge plates with the thickness of 100 μm and 200 μm attached to two copper electrodes are shown in Figure 3(a, b), respectively. With electrical resistance of 16.4 Ω and 8 Ω the sponges can withstand several amps of electrical current in air. The fabrication process is simple and low-cost, involving polymethyl-methacrylate (PMMA) microspheres as a template and polyacrylonitrile (PAN) as a precursor to create crosslink between MWNTs [19]. The density of sponges varies from 10 to 36 mg/cm^3. The sponge maintains a stable performance after 1000 large strain compression cycles.

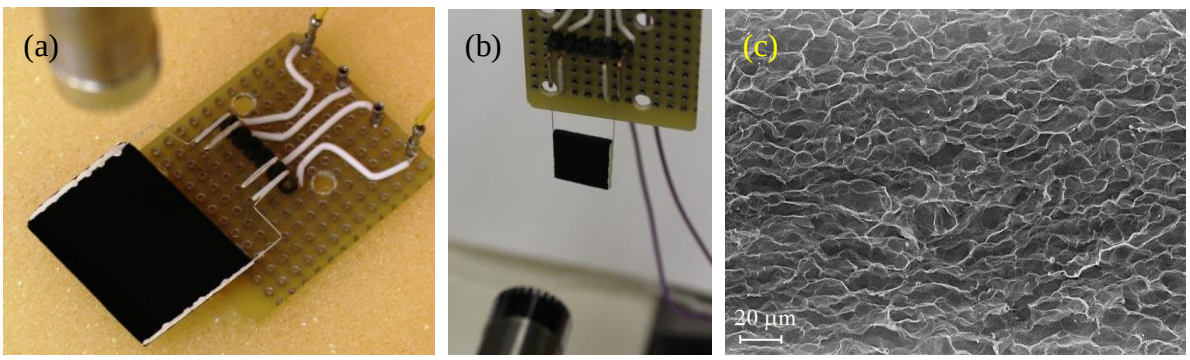

Figure 3. (a, b) Pictures of (2x2.5 cm^2) and (1.5x1.5 cm^2) MWNT sponge plates with thickness of 100 μm and 200 μm, respectively. (c) SEM image of the sponge with density of 30 mg/cm^3.

The porosity and the pore size of the CNT foam can be tuned easily by adjusting the concentration and particle size of the PMMA spheres. The MWNT sponges have a hierarchically porous structure and the pore size ranges from several nanometers to tens of micrometers, Figure 3(c).

Unlike the CVD grown freestanding MWNT forest the MWNT sponge shows $p_{rms} \sim f^{0.6}$ dependence which is typical for TA system with substantial contribution of heat capacity of the heater (Figure 4(a)). Apparently, the collapse of individual CNTs into large bundles, unavoidable in such technology, increases the volumetric heat capacity and thermal inertia of the heater. On the other hand, the smaller plate thickness and better heat transfer to the gas through large (~10-20 μm) pores result in higher sound pressure from this heat source at low frequencies. The thinner plates would be preferable to avoid the heat accumulation as indicated in $p_{rms}(P_h)$ plot of Figure 4 (b) as a deviation from the linear increase. Our results show that CNT sponges have the potential to fabricate elastic deformable TA sound transducers with enhanced performance.

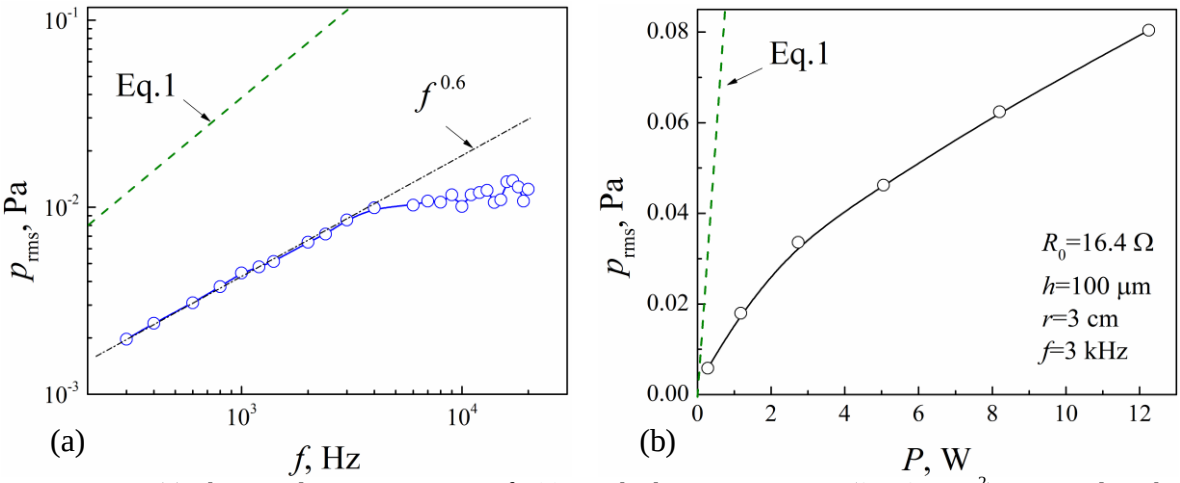

Figure 4. (a) The sound pressure spectra of 100 μm thick MWNT sponge (3.5x3.5 cm^2) measured on the distance of 3 cm in open air at T_0=25 °C. The sound pressure is normalized to the applied ac power, P_h=1.17 W. The green dashed line show the theoretical line according to Eq.1. (b) The sound pressure versus applied ac power (open blue circles) measured on the distance r = 3 cm, f = 3 kHz.

2.3 Graphene sponge.

The specific surface area of ultra-thin two-dimensional (2D) graphene film is limited. In order to utilize the high inherent properties of graphene, such as high electronic conductivity, good thermal stability, and excellent mechanical strength, recently porous graphene materials including graphene nanomesh, crumpled graphene and graphene foam have attracted tremendous attention and research interest, owing to their exceptional surface area, and high pore volume [20].

The studied here three-dimensional (3D) cross-linked graphene sponge was fabricated by solvothermal (ST) reaction in alcohol [21, 22]. This essentially isotropic graphene sponge has air-like density and demonstrates highly repeatable compression. Graphene oxide (GO) sheets are first ST assembled in ethanol to obtain a nearly homogenous, ethanol-filled material. Following exchange of ethanol with water, the sponge is freeze-dried and then annealed under inert atmosphere at 400°C to obtain the final graphene sponge (GS). By varying the GO concentrations used for the ST reaction, GS possessing densities from 0.3 to 14 mg/cm^3 were obtained, which in the former case have a much lower density than ambient air (1.2 mg/cm^3). The results discussed below are for GS having an uncompressed density of 14 mg/cm^3.

The thin slices of graphene sponge, along and perpendicular to the cylinder axis shown in figure 5(a), were cut by laser beam at ambient conditions. The thermal conductivity of GS, obtained as a product of measured thermal diffusivity (Angstrom method), heat capacity and density, $\lambda=\rho C_p \alpha=0.016 \pm 0.002$ W/mK, is two times lower than the thermal conductivity of air, 0.026 W/mK. The fine microscopic structure of GS demonstrates essentially isotropic heat conduction, independent of the cutting direction (α_{II} =2.25 mm^2/s, $\alpha_{\perp}$=2.31 mm^2/s).

For testing the TA performance of GS heaters, three samples cut parallel (1.5x12.5x15 mm^3, 1x10x15 mm^3) and perpendicular (0.8 mm thick and 18 mm in diameter) to the cylinder axis were fabricated. Despite large thicknesses, the studied GS show linear frequency dependencies of sound pressure (Figure. 6(a)) with sound pressure close to the theoretical level at low applied power, P_h<0.5 W. The linear $p_{rms}(f)$ indicates a low heat capacity of individual heater constituents (graphene sheets), which is lower than the heat capacity of surrounding air. This is consistent with our density and heat capacity measurements.

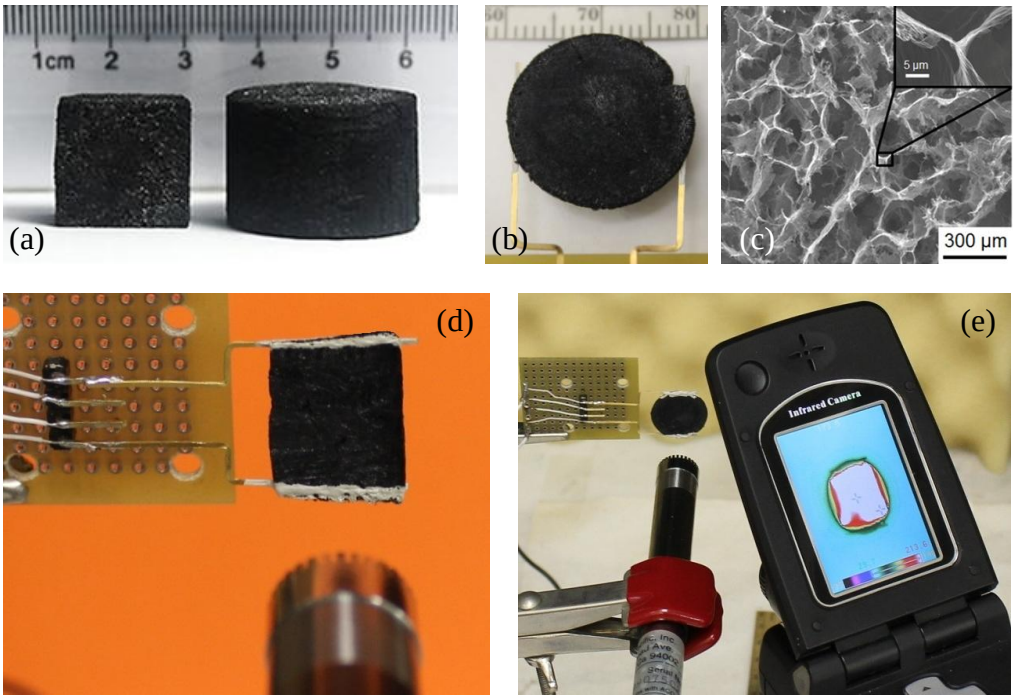

Figure.5 (a) The picture of GS cylinders fabricated by solvothermal reaction. (b) 0.8 mm thick plate, made by laser cutting perpendicular to the cylinder axis, attached to the gold coated electrodes by silver paste. (c) SEM image of the sponge with the density 14 mg/cm^3. (d) 1.5 mm thick GS plate cut parallel to the cylinder axis placed 3 cm from the microphone (model 7046). (e) Infrared camera MobIR with preinstalled emissivity of 0.98 shows the temperature on the surface of TA heater.

However, further increase of P_h creates the accumulation of heat inside of closed voids and causes a decline in the $p_{rms}(P_h)$ curve. To improve the efficiency of GS heaters, the thinner plates with fully accessible voids are desired. The further work on enhanced bounding between graphene flakes is necessary to fabricate mechanically strong thin films with high electronic conductivity.

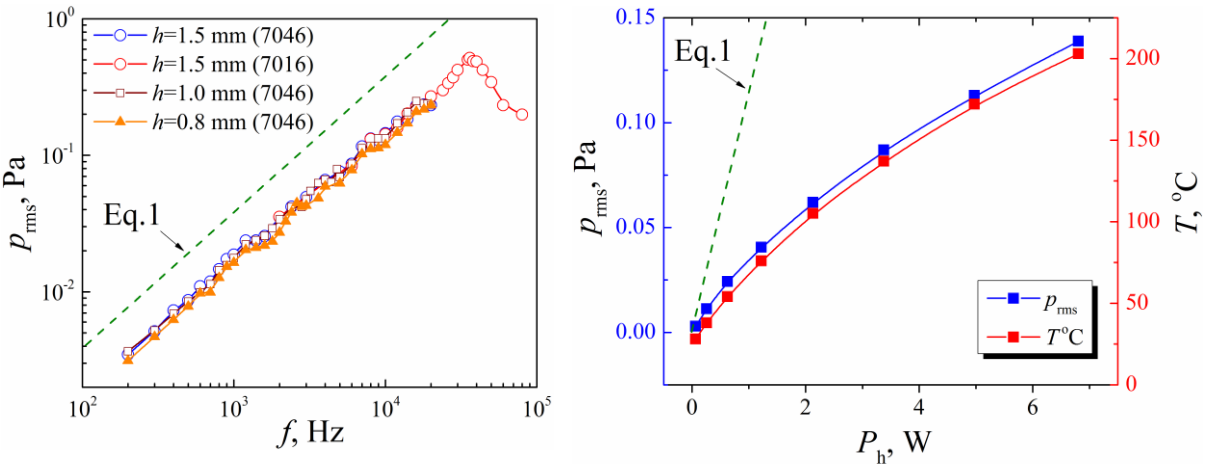

Figure 6. (a) The sound pressure spectra of 0.8 mm (solid orange triangles), 1 mm (open wine square), and 1.5 mm (open blue circles) thick GS sponges measured at a distance of 3 cm in open air at T_0 = 25 °C. The numbers in parenthesis show the used microphone model. The sound pressure is normalized to the applied ac power. The green dashed line show the theoretical line according to Eq. (1). (b) The sound pressure versus applied ac power (solid blue squares) measured at the distance r = 3 cm, f = 3 kHz. The temperature of GS sponge (h=0.8 mm, D=18 mm) versus applied power (solid red squares) was measured using infrared camera MobIR.

2.4 Gold coated Poly(acrylonitrile) (PAN) sheets

PAN $(C_3H_3N)_n$ which is a polymer with a chain of carbon connected to one another is durable, strong, relatively insoluble, and a high-melting temperature material [23]. Electrospun PAN sheets, shown in Figure 7 (a) with fiber diameters between 200-500 nm, can withstand relatively high temperatures in air (T_m=317 ^oC). Taking into account the low thermal expansion coefficient (~6.6 x 10^{-5}/K), the highly aligned sheet coated with a thin ~100 nm metallic film can be considered as a good candidate for TA sound projectors. The diameter of individual fibers, the thickness of PAN sheet, and the density can be easily controlled by precursor solution (10 wt% of Polyacrylonitrile, (M_w = 150,000) in N,N-dimethylacetamide, Sigma-Aldrich), applied voltage, distance to counter electrode and spinning time [23].

The gold coated sheets with electrical resistances of 532 Ω and 16 Ω, for low and high density PAN sheets, respectively, are optically transparent (T_{low} > 95 %), mechanically robust and does not create macroscale bundles. The metallic film as a 100 nm shell on individual fibers was deposited by RF-sputtering (DC/RF Reactive Magnetron Sputter, ATC Orion).

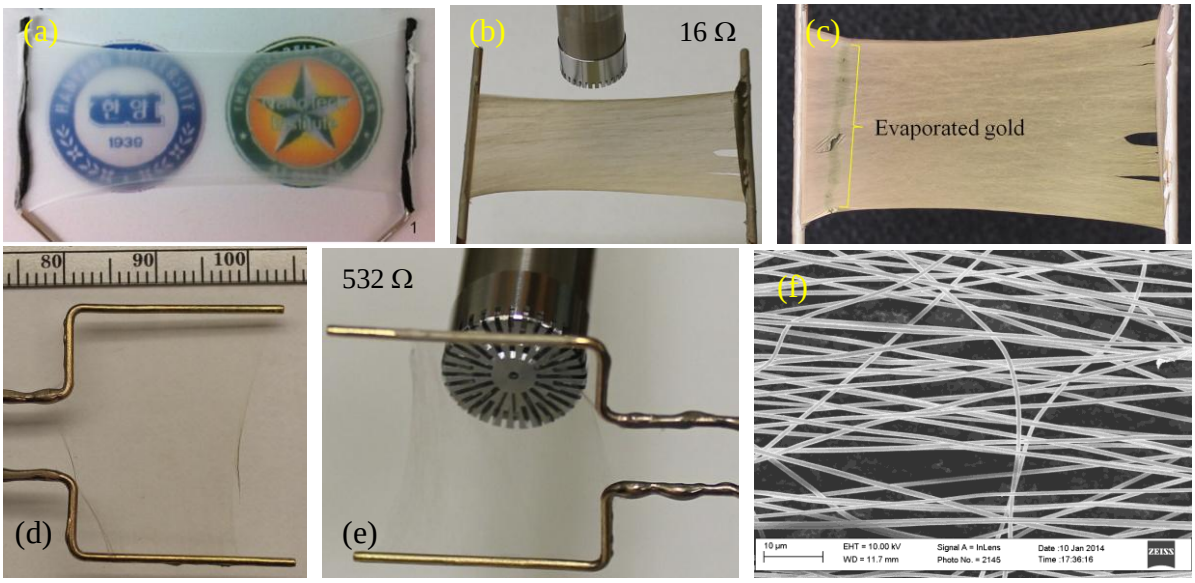

Figure 7. (a) The PAN sheet electrospun between two metallic electrodes. Logos of Hanyang University, Seoul and NanoTech institute, UTDallas are visible through the sheet. (b) The dense gold coated PAN sheets (R=16 Ω) placed of the distance of 3 cm from the microphone. (f) The sheet of Fig.7(c) after applying 0.7 A. (d, e) The thin, transparent gold coated PAN sheets (R=532 Ω) with optical transparency > 95%. (f) The SEM image of the gold coated PAN sheet.

The aerogel density sheet shown in Figure 7(e) demonstrates an excellent TA heat source performance up to 40 kHz. The little reduced slope of sound pressure dependence versus sound frequency, p_{rms}~$f^{0.8}$ and lower cut off frequency (~40 kHz) indicate the increased volumetric heat capacity of the sheet compared to the heat capacity of air. Despite of high thermal inertia of large in diameter PAN fibers (400-600 nm),

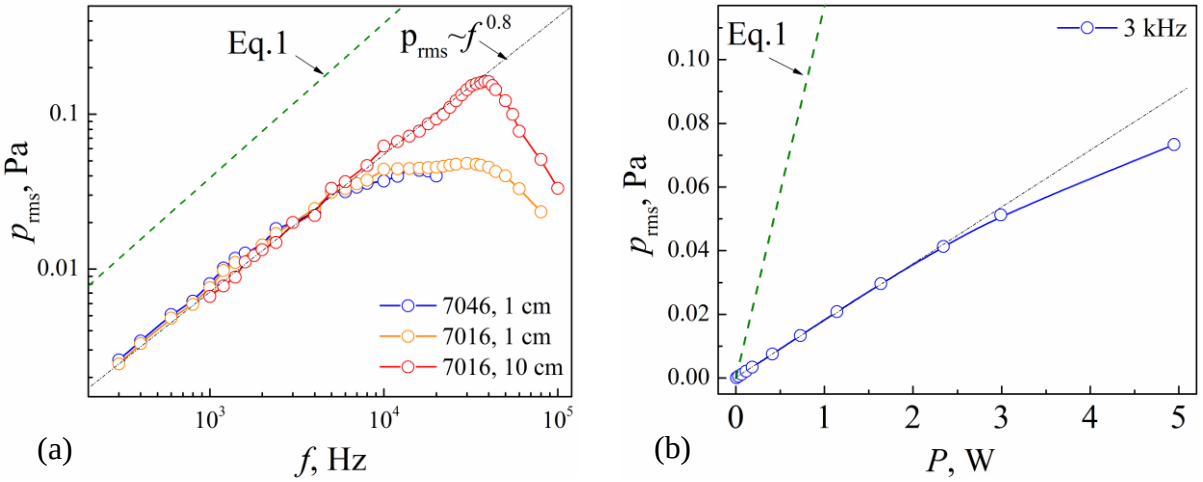

Figure 8. (a) The sound pressure spectra of gold coated (2.5x2.5 cm^2) PAN sheet measured on the distance r=1 and 10 cm, respectively in open air at T_0=25 ^oC. The sound pressure is normalized to the applied ac power, P_h=0.72 W. Open blue circles show the $p_{rms}(f)$ response measured using precision condenser microphone model 7046, (2 Hz–20 kHz) at a distance 1 cm and open orange circles, using model 7016, (5 Hz–120 kHz) and open red circes using model 7016 (ACO Pacific, Inc) on the distance 10 cm. The green dashed line show the theoretical line according to Eq.1 for the distance 3 cm. (b) The sound pressure versus applied ac power (open blue circles), f=3 kHz. The temperature on the surface of heater measured by infrared camera did not exceed 35 ^oC. All plots normalized to the distance of 3 cm.

which decreases the overall performance of TA heater, the open aerogel structure of the Au/PAN sheet provides enhanced heat exchange and a linear power dependence of sound pressure. The $p_{rms}(P_h)$ for 532 Ω thin sheet (Figure 7(d, e)) taken at 3 kHz shows 6 fold lower slope, but enhanced power limit (Figure 8(b)). Partial pyrolysis of PAN sheet in inert gases, preserving the mechanical strength and decreasing the fiber diameter is promising route to improve the performance of TA heater. The 3x7 cm^2 gold coated sheet shown in Figure 7(b), which has a higher density and lower resistance (16 Ω), shows relatively lower performance. Surprisingly, at applied ac current of 0.7 A (~8 W) the gold film was suddenly evaporated at bottleneck line (shown in Figure 7(c) as a grey line) at relatively low temperatures, ~300 ^oC. Note, the PAN sheet under the coating is partially carbonized and survived. Further study of gold coated PAN sheets show strong tendency of thin Au film with nanoscaled grain structure to melt and evaporate at relatively low temperatures on the surface of TA heater.

2.5 Indium-tin oxide coated PAN sheets

PAN fibers coated with indium tin oxide (ITO) film also show very promising results. First, the ITO film can withstand oxygen environment at relatively high temperatures. Second, it is highly conductive and transparent. Finally, it has positive TCR.

The tin-doped indium oxide ($In_{2-y}Sn_yO_{3-\delta}$, y~0.1) also well known as indium-tin oxide (ITO) was deposited by rf-sputtering (1% O_2 in Ar carrier gas, flow rate 12 cm^3, 4 mTorr). The thickness of as deposited ITO films estimated from SEM images varied between 100-110 nm. All samples were annealed after deposition in air at T_{an}=250 ^oC for 1 hour.

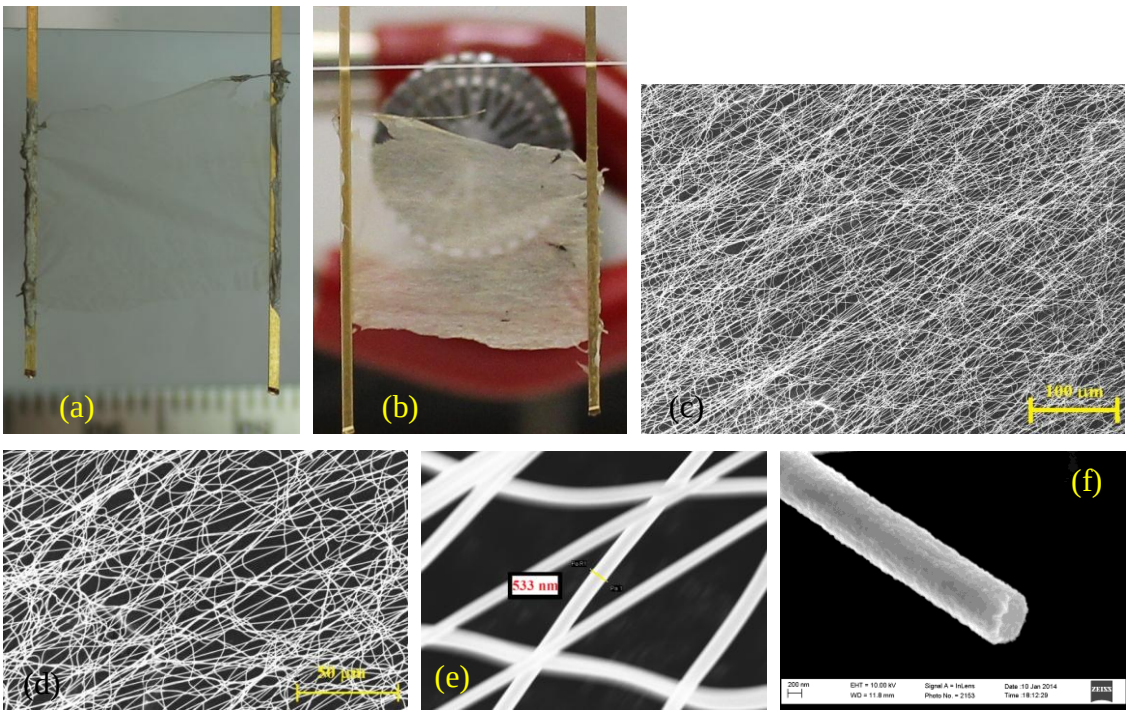

Figure 9. (a, b) The pictures of pristine ITO-coated PAN sheet and ITO sheet with burned out PAN fibers. (c, d, e) The SEM image of the ITO coated PAN sheet and individual fibers. (f) The hollow ITO tube after resistively heated and burned PAN core.

The SEM images of figure 9 (c-f) show the aligned, partially weaved structure of ITO coated PAN fibers with average diameter of ~400-500 nm without any trace of bundling. The length of individual fibers is the distance between electrodes; therefore, the sheet does not suffer on interconnects resistance, which occurs in MWNT sheets with the length of individual carbon nanotubes of 250-300 μm. The thermal conductivity of individual fibers is relatively small (3-4 W/mK) due to low conductivity of core PAN fibers (0.05 W/mK) and nanostructured thin ITO film. The organic PAN core can be burned out in air by applying ac current. The Figures 9(a, b) show the same sheet before and after burning. The tubular structure of ITO fiber is shown in Figure 9(f). Despite of low electrical conductivity, a single-side coated PAN sheet demonstrates good TA heater performance with the spectral slope $\sim f^{0.7}$. Sheets coated on both sides show a reduced spectral slope, $\sim f^{0.53}$ and power dependence of sound pressure (Figure 10 (a, b)). Thus, the increase in the fiber diameter and the thickness of conductive layer shifts the slope of sound pressure spectra from 1.0 (the heat capacity of the surrounding gas is dominates) to 0.5 (the heat capacity of the heater is dominates). This tendency is consistent with above thermodynamic model of thermoacoustic transduction. More works is need to reduce the diameter of conductive fibers at least to 50 nm. The open aerogel structure of ITO/PAN sheet provide excellent heat exchange conditions resulting in linear power dependence slope up to 5 W/cm^2, which is close to the power limit of free-standing single MWNT sheet [18].

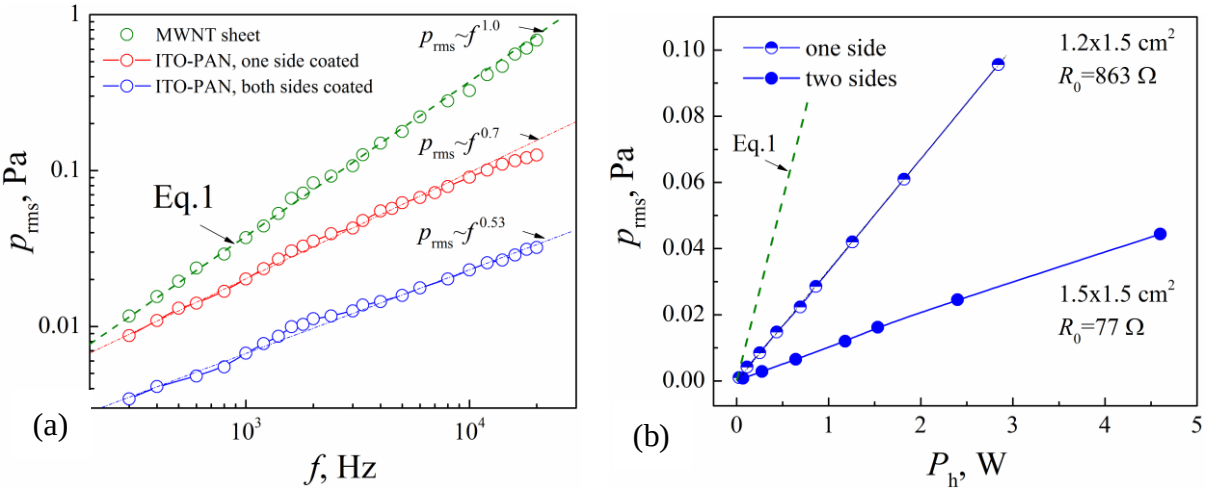

Figure 10. (a) The sound pressure spectra of ITO coated PAN sheet shown in Figure 9 (a): The red open circles are for one side coated sheet (1.2x1.5 cm^2, R=863 Ω, P_h=0.3 W), blue open circles are for both side coated sheet (1.2x1.5 cm^2, R=77 Ω, P_h=0.29 W), r=3 cm. The spectra of single layer MWNT sheet (green open circles), (1.2x1.5 cm^2, R=1980 Ω, P_h=0.24 W), and the theoretical line (green dashed line) are shown for comparison. (b) The sound pressure versus applied ac power measured on the distance of 3 cm at f=3 kHz for single-side coated sheet (half-filled blue circle) and two-side coated sheet (solid blue circles), respectively.

3. CONCLUSIONS

Bulk samples of carbon nanotube aerogels exhibit fascinating behavior, including highly anisotropic electrical and thermal transport properties and a higher specific strength than the strongest steel sheet. The invention of dry-state technology to fabricate free-standing MWNT sheets has resulted in many verious promising applications. The thermoacoustic sound generation is one of them, which fully exploits amazing properties of CNTs. However, the limited access to this complex technology is frustrating and hampers the field. Here I have demonstrated several alternative structures exhibiting good thermoacoustic performance as a heat source with desirable functionalities. The sample preparation technologies for these structures are well established and described in detail in literature. I have studied the thermoacoustic performance of these thin structures as a heat source, or as a heat source support for TA sound generation. The slope of frequency and power dependencies help characterize the thermoacoustic performance of these structures. The better TA performance demonstrate 3D nanostructures with larger surface area accessible for the heat exchange with surrounding medium. 2D nanostructures, such a graphene film, ITO, or other conductive polymer films show much (more than one order) lower sound pressure. The thin, flexible and transparent for optical and acoustical waves 3D films can be easily diploid on any curved surfaces and serve as a thermoacoustic heat source for SONAR systems and noise cancelation.

ACKNOWLEDGEMENTS

I thank Monica Jung de Andrade (NanoTech Institute, UT Dallas), Raquel Ovalle Robles (Nano-Science & Technology Center, Lintec of America, Inc.), Jae Ah Lee (Hanyang University, Seoul) for ITO/PAN sample preparation and providing drawable MWNT forests, Mei Zhang (Florida State University) for CNT sponge and Yongsheng Chen (Nankai University, Tianjin, China) for Graphene sponge samples and fruitful discussion. This research work was supported by Office of Naval Research grants N00014-14-1-0152, N00014-13-1-0180, Air Force Office of Scientific Research grant FA9550-12-1-0211, and the Robert A. Welch Foundation Grant AT-0029.

REFERENCES

1. Xiao L, Chen Z, Feng C, Liu L, Bai Z-Q, Wang Y, Qian L, Zhang Y, Li Q, Jiang K, and Fan S. Flexible, stretchable, transparent carbon nanotube thin film loudspeakers. Nano Lett. 2008; 8: 4539–4545.
2. Aliev AE, Lima MD, Fang S, Baughman RH. Underwater sound generation using carbon nanotube projectors. Nano Lett. 2010; 10:2374-2380.
3. Xiao L, Liu P, Liu L, Li Q, Feng Zh, Fan Sh, Jiang K. High frequency response of carbon nanotube thin film speaker in gases. J. Appl. Phys. 2011;110: 084311.
4. Aliev AE, Gartstein YN, Baughman RH. Increasing the efficiency of thermoacoustic carbon nanotube sound projectors. Nanotechnology. 2013;24:235501.
5. Vesterinen V, Niskanen AO, Hassel J, Helistö P. Fundamental efficiency of nanothermophones: Modeling and experiments. Nano Lett. 2010;10(12):5020–5024.
6. Tong LH, Lim CW, Li YC. Gas-filled encapsulated thermal-acoustic transducer. ASME J. Vibr. Acoust. 2013;135(5): 051033.
7. Tian H, Ren T-L, Xie D, Wang Y-F, Zhou C-J, Feng T-T, Fu D, Yang Y, Peng P-G, Wang L-G, Liu L-T. Graphene-on-paper sound source devices. ACSNano 2011;5(6): 4878–4885.
8. Suk JW, Kirk K, Hao Y, Hall NA, Ruoff RS. Thermoacoustic sound generation from monolayer graphene for transparent and flexible sound sources. Adv. Mater. 2012;24(47):6342–6347.
9. Tian H, Xie D, Yang Y, Ren T-L, Feng T-T, Wang Y-F, Zhou C-J, Peng P-G, Wang L-G, Liu L-T. Poly(3,4-ethylenedioxythiophene):poly(styrenesulfonate)-based organic, ultrathin, and transparent sound-emitting device. J. Appl. Phys. 2011;99:233503.
10. Shinoda H, Nakajima T, Ueno K, Koshida N. Thermally induced ultrasonic emission from porous silicon. Nature 1999;400:853–855.
11. Niskanen AO, Hassel J, Tikander M, Maijala P, Grönberg L, Helistö P. Suspended metal wire array as a thermoacoustic sound source. Appl. Phys. Lett. 2009; 95:163102.
12. Tian H, Xie D, Yang Y, Ren T-L, Wang Y-F, Zhou C-J, Peng P-G, Wang L-G, Liu L-T. Transparent, flexible, ultrathin sound source devices using indium tin oxide films. Appl. Phys. Lett. 2011;99: 043503.
13. Zhang M, Fang SL, Zakhidov AA, Lee SB, Aliev AE, Williams CD, Atkinson KR, Baughman RH. Strong, transparent, multifunctional, carbon nanotube sheets. Science 2005;19:1215–19.
14. Chitnis G, Kim A, Song SH, Jessop AM, Bolton JS, Ziaie B. A thermophone on porous polymeric substrate. Appl. Phys. Lett. 2012;101:021911.
15. Sugimoto T, Nakajima Y. Acoustic characteristics of a flexible sound generator based on thermoacoustic effect, Proc ICA meetings on Acoustics, Engineering Acoustics Session 1aEA: Thermoacoustics I, 19, 2013.
16. Arnold HD,Crandall IB. The thermophone as a precision source of sound. Phys. Rev. 1917;10:22–38.
17. Kozlov ME, Haines CS, Oh J, Lima MD, Fang S. Sound of carbon nanotube assemblies. J. Appl. Phys. 2009;106:124311.
18. Aliev AE, Mayo NK, Baughman RH. Avirovik D, Priya S, Zarnetske MR, Blottman JB. Thermal management of thermoacoustic sound projectors using a free-standing carbon nanotube aerogel sheet as heat source. Nanotechnology 2014; 500085/PAP/207298.
19. Cui Y, Zhang M. Fabrication of cross-linked carbon nanotube foam using polymethylmethacrylate microspheres as templates. J. Mater. Chem. A 2013;1:13984-13988.
20. Jiang L, Fan Zh. Design of advanced porous graphene materials: from graphene nanomesh to 3D architectures. Nanoscale. 2014;6:1922-1945.
21. Bi H, Yin K, Xie X, Zhou Y, Wan N, Xu F, Banhart F, Sun L, Ruoff RS. Low temperature casting of graphene with high compressive strength. Advanced Materials. 2012;24(37): 5124-5129.
22. Zhang L, Zhang F, Yang X, Long G, Wu Y, Zhang T, Leng K, Huang Y, Ma Y, Yu A, Chen Y. Porous 3D graphene-based bulk materials with exceptional high surface area and excellent conductivity for supercapacitors. Scientific Reports. 2013;3:1408.
23. Rahaman MSA, Ismail AF, Mustafa A. A review of heat treatment on polyacrylonitrile fiber. Polymer Degradation and Stability. 2007; 92:1421-1432.